

COMMUNICATION

[View Article Online](#)
[View Journal](#) | [View Issue](#)



Cite this: *Nanoscale Adv.*, 2023, **5**, 1910

Received 14th June 2022

Accepted 8th November 2022

DOI: 10.1039/d2na00378c

rsc.li/nanoscale-advances

Antibiotic resistance combined with pathogen internalization leads to debilitating infections. Here we test novel superoxide producing, stimuli-activated quantum dots (QDs), to treat an intracellular infection of *Salmonella enterica* serovar Typhimurium in an osteoblast precursor cell line. These QDs are precisely tuned to reduce dissolved oxygen to superoxide and kill bacteria upon stimulation (e.g., light). We show QDs provide tunable clearance at various multiplicities of infection and limited host cell toxicity by modulating their concentration and stimuli intensity, proving the efficacy of superoxide producing QDs for intracellular infection treatment and establishing a framework for further testing in different infection models.

The rapid emergence of multi drug resistant (MDR) infectious diseases has created a global health crisis which is made worse by the decreasing pipeline of new antimicrobial therapies in production.^{1–5} In the United States, as reported by the Center for Disease Control in 2019, there are more than 2.8 million antibiotic-resistance infections each year and more than 35 000 deaths.⁶ Compounding the emergence of MDR bacteria is bacteria's ability to evade treatment by residing intracellularly within host cells. By hiding intracellularly, bacteria create multiple physical barriers to treatment: the host cell membrane, any intracellular vacuole, and the bacteria membrane.⁷ Antibiotics such as β -lactams, aminoglycosides, fluoroquinolones, and macrolides have little or no efficacy in treating intracellular infections due to poor transport into host cells, low retention in host cells, or decreased intracellular concentrations due to the host cell environment.^{7–9} Due to these

compounding issues a novel solution to treat infectious disease is desperately needed.

One solution is to mimic the body's natural defense mechanism. Within the innate immune system macrophages, neutrophils, and dendritic cells eliminate intracellular infections through phagocytic respiratory burst. Respiratory burst clears intracellular infections by generating a lethal bolus of the reactive oxygen species (ROS) superoxide (O_2^-).^{10,11} This toxic dose of superoxide induces oxidative stress causing DNA damage, protein damage, and eventually lysis.^{11–14} Additionally, perturbing ROS concentrations is an effective extracellular antimicrobial as many antibiotics induce oxidative stress, including aminoglycosides, quinolones, rifampicin, and chloramphenicols.¹⁵

While most therapeutics are effective at eliminating extracellular bacteria, here we expand on bacteria's sensitivity to ROS perturbations by utilizing superoxide-producing quantum dot (QD) nanoparticles to treat an intracellular infection. Unlike numerous antibiotics, studies show that nanoparticles have enhanced transport into mammalian cells and are more effective at treating intracellular infections compared to small molecules alone.^{16–18} Further, we have shown that superoxide specific generation offers the largest therapeutic window when comparing different ROS,¹⁹ while still eliminating bacteria at nanomolar concentrations without showing toxicity in different mammalian cell lines^{20–23} or a murine model,²⁴ the latter of which showed robust renal clearance of CdTe-2.4 eV QDs with no deleterious effects to host organ systems. Combining the superior transport of these nanoparticles and superoxide's large therapeutic window creates an ideal treatment for intracellular infections.

Quantum dots (QDs) are semiconductor nanoparticles that have tunable quantum states based on their size, shape, and material, conferring specific reduction and oxidation potentials.^{25,26} Based on their specific reduction potential, QDs can react with surrounding molecules upon activation by a stimulus. They do so by utilizing the provided stimuli to activate an electron across their bandgap, creating an electron hole pair

^aChemical and Biological Engineering, University of Colorado Boulder, Boulder, CO 80303, USA. E-mail: chatterjee@colorado.edu

^bRenewable and Sustainable Energy Institute, University of Colorado Boulder, Boulder, CO 80303, USA

^cSachi Bioworks Inc., Colorado Technology Center, Louisville, CO 80027, USA

^dAntimicrobial Regeneration Consortium Labs, Louisville, CO, 80027, USA

† Electronic supplementary information (ESI) available. See DOI: <https://doi.org/10.1039/d2na00378c>



which, based on the redox potential, can react with available molecules nearby. Here we use light activated cadmium telluride QDs (~ 3 nm in diameter) tuned to a bandgap of 2.4 eV, a redox potential specific to reduce dissolved oxygen to superoxide.²⁷⁻³⁰ By being stimuli-activated these therapeutic nanoparticles also provide spatial and temporal control, providing opportunities to negate the negative effects of broad-spectrum antibiotics that eliminate infectious and beneficial bacteria throughout the body and unnecessarily expose all bacteria, increasing the likelihood of resistance to develop.

Here we test our superoxide producing nanoparticles in treating a bone intracellular infection model, specifically a *Salmonella* infection of preosteoblast cells. Osteomyelitis, bacterial infection of bone, is devastating and difficult to treat as it is known to be chronic, reoccurring, and often refractory to antibiotics due to the dense matrix of bone and internalization of bacteria. Osteomyelitis can require long-term (6–18 months) antibiotic treatment, surgical debridement, and amputation, and has high rates of treatment failure leading to bone loss and death.^{31,32} Specifically, *Salmonella enterica* serotype Typhimurium causing osteomyelitis has a high incidence rate in patients with Sickle Cell Disease and is known to infect intracellularly, creating further physical barriers for treatment.^{33,34} The combined rise in MDR infections and osteomyelitis' difficult treatment and devastating outcomes warrant novel solutions. Given the severity of osteomyelitis and its uniquely challenging treatment, we selected preosteoblast cells for our model as a proof of concept for translation of our treatment to a variety of elusive intracellular infections (such as gastrointestinal or dermal infections). Here we investigate the use of superoxide producing nanoparticles as a therapy for the hard to treat and hard to reach intracellular infections.

Prior to testing an intracellular infection treatment of *Salmonella enterica* serovar Typhimurium strain SL1344, the toxicity of our superoxide specific generating nanoparticles was validated extracellularly. These 3 nm, cadmium telluride, semiconducting nanoparticles are rationally designed to achieve a 2.4 eV band gap, that upon light activation generates an electron-hole pair at the precise reduction potential to convert dissolved oxygen to superoxide (Fig. 1A, left). The reduction potential is specific to the material properties and size (correlated to band gap distance); as such the same cadmium telluride nanoparticle at a different size, and therefore smaller band gap of 2.2 eV, does not produce superoxide because its conduction band is no longer above molecular oxygen's reduction potential (Fig. 1A, right). Superoxide producing CdTe-2.4 eV emits green light and CdTe 2.2 eV emits red light, therefore, figures using CdTe-2.4 eV are shown in green and figures using CdTe 2.2 eV are shown in red. Superoxide production was validated using electro paramagnetic resonance (EPR) spectroscopy (Fig. 1B and ESI Fig. S1†), where we see superoxide production as well as hydroxyl adducts from immediate superoxide dismutation to hydroxyl radicals. Normalized superoxide production shows a significant reduction in superoxide productions between CdTe-2.4 eV and CdTe 2.2 eV (two sample *t*-test, $P < 0.001$). Due to the wider size distribution of CdTe-2.2 eV as compared to the CdTe-2.4 eV (ESI Fig. S1†), there is

a small portion of nanoparticles at the correct size to produce superoxide; therefore, superoxide production is not eliminated completely but reduced to 20% that of the CdTe-2.4 eV QDs.

Superoxide specific toxicity of *Salmonella* was tested by microdilution in broth culture to a 1 : 1000 dilution from overnight culture followed by 18 hours of growth with or without light activation (Fig. 1C). Bacterial optical density normalized to no treatment shows that with the addition of CdTe-2.4 eV nanoparticles causes no significant reduction in growth (two sample *t*-test, $P > 0.05$) without light activation (dark), and therefore no superoxide production, at 100, 400, or even 600 nM (Fig. 1F). Upon light activation a concentration dependent growth reduction is seen at all three concentrations, indicating a superoxide specific dependence on bacterial toxicity (Fig. 1D and F, two sample *t*-test, $P < 0.05$). The addition of light shows no toxicity as seen by comparing no nanoparticle treatment in light and dark conditions (ESI Fig. S2†). Further validation used CdTe 2.2 eV as a superoxide specific toxicity control while maintaining the same materials and incorporating light illumination. Upon treatment with light activated CdTe-2.2 eV the growth inhibition is significantly less than that of the CdTe-2.4 eV at 100, 400, and 600 nM, and no growth inhibition in dark conditions (Fig. 1E and G).

With an established toxicity threshold determined for extracellular *Salmonella*, we established the toxicity threshold for the preosteoblast host cells in our intracellular infection model to verify a therapeutic window. Reactive oxygen species can be toxic to mammalian cells but at higher concentrations than typically seen for bacteria.²⁷ Here we confirm that by measuring the viability of the osteoblast precursor cells after 18 hours of treatment with CdTe-2.4 eV under light activation (Fig. 2A). Osteoblast precursor cells were allowed to adhere for 24 hours prior to addition of QD nanoparticles at an initial seeding density of 10 000 cells per well in a 96-well plate. Viability was measured using a resazurin metabolic assay which is converted to the fluorescent molecule resorufin by the metabolism of viable cells. Percent viability was determined by normalizing fluorescence to no treatment. No toxicity was seen up to 1 μ M of CdTe-2.4 eV under light activation (Fig. 2B, ESI Fig. S3 & S4† two sample *t*-test, $P > 0.05$).

Prior to testing the therapeutic efficacy of superoxide producing nanoparticles as a *Salmonella* intracellular infection treatment, we established and characterized the intracellular infection of *Salmonella* in preosteoblast cells. The preosteoblast cells were seeded at 10 000 cells per well in a 96 well plate and allowed to adhere for 24 hours prior to infection (Fig. 3A). Before infection, *Salmonella* was grown overnight, diluted 1 : 10, regrown for 3 hours, and added to the preosteoblast cells at the desired multiplicity of infection (MOI). The CFU per mL of *Salmonella* was determined using optical density at 600 nm and a previously determined linear calibration (ESI Fig. S5†). After allowing 45 minutes for the *Salmonella* to infect, the media was replaced with preosteoblast growth media containing gentamicin for 75 minutes. Gentamicin is an antibiotic that cannot enter eukaryotic cells and thereby kills the extracellular bacteria while maintaining an intracellular infection.³⁵ The media was then replaced to remove any dead extracellular bacteria and



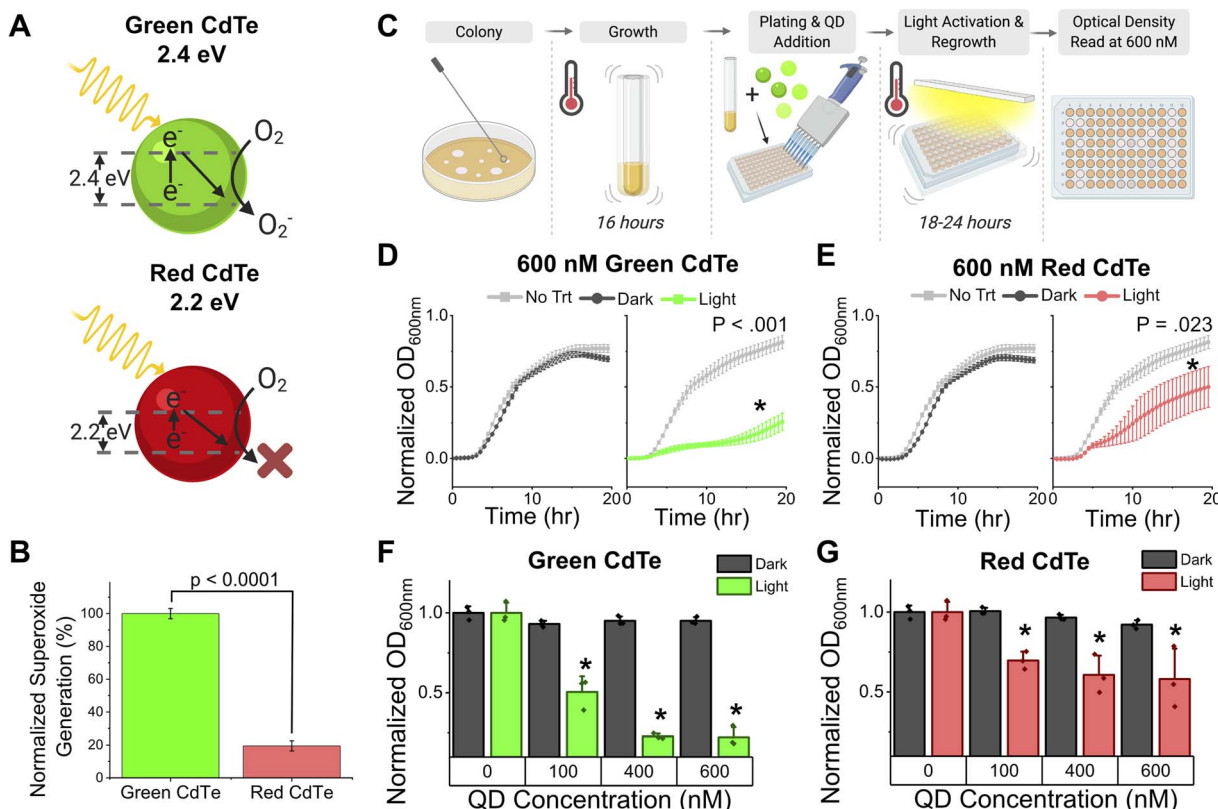


Fig. 1 Superoxide specific bacterial toxicity. (A) CdTe nanoparticles synthesized at different bandgap sizes, 2.4 eV and 2.2 eV, where the green emitting CdTe produces superoxide and the red emitting CdTe does not. (B) EPR showing significant reduction in superoxide generation between green and red CdTe. (C) Bacterial growth assay scheme with nanoparticle and light activation treatment. (D) Growth curve (20 hours) of *Salmonella* treated with 600 nM CdTe-2.4 eV in dark (left) and light activation (right). (E) Growth curve (20 hours) of *Salmonella* treated with 600 nM CdTe 2.2 eV in dark (left) and light activation (right). (F) Optical density, 600 nm, at 18 hours of treatment condition normalized to no treatment condition for CdTe-2.4 eV. Significant reduction (t -test, unpaired, equal variance, $\alpha = 0.05$) was seen in all CdTe-2.4 eV light activation conditions and not in dark. (G) Optical density, 600 nm, at 18 hours of treatment condition normalized to no treatment condition for CdTe 2.2 eV. Significant reduction (t -test, unpaired, equal variance, $\alpha = 0.05$) was seen in all CdTe 2.2 eV light activation conditions and not in dark at 16 hours of growth. The reduction due to light activation with CdTe 2.2 eV is much less than was CdTe-2.4 eV.

incubated for 18 hours in gentamicin containing media to retain the intracellular infection.

First, the infection was characterized by varying the MOI and enumerating the colony forming units (CFU) within the pre-osteoblast cells at the end of 18 hours of incubation by lysing the host mammalian cells (Fig. 3A). The infected MOI varied

from 12 (± 8.5) to 155 (± 7.1) ($1.2 \times 10^6 \pm 8.5 \times 10^5$ to $1.55 \times 10^7 \pm 7.1 \times 10^5$ CFU per mL) and showed a linear trend in the lysed CFU per mL compared to the infected CFU per mL up to an MOI of 79 (± 11.3) where the linear trend no longer seemed to hold ($R^2 = 0.875$). At 155 MOI the associated lysed CFU per mL decreased and did not follow the linear trend ($R^2 = 0.832$),

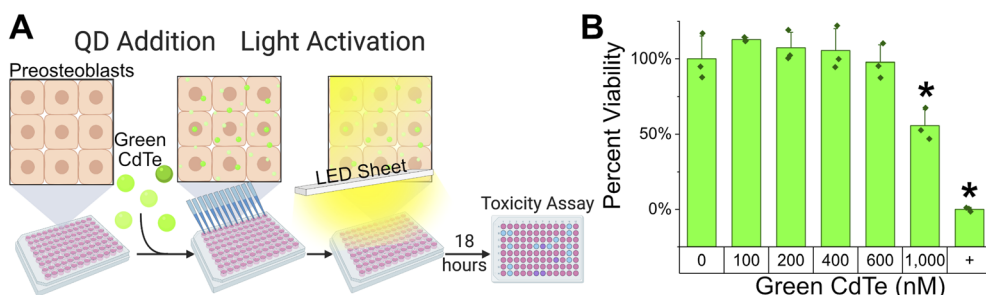


Fig. 2 Nanoparticle toxicity threshold in preosteoblast. (A) Schematic of toxicity testing protocol of CdTe-2.4 eV in preosteoblast cells with light activation. (B) Resazurin assay results of preosteoblast cell viability after 18 hours of CdTe-2.4 exposure with light activation. Statistically significant toxicity seen at 1 μ M CdTe-2.4 eV (unpaired t -test, equal variance, $\alpha = 0.05$).

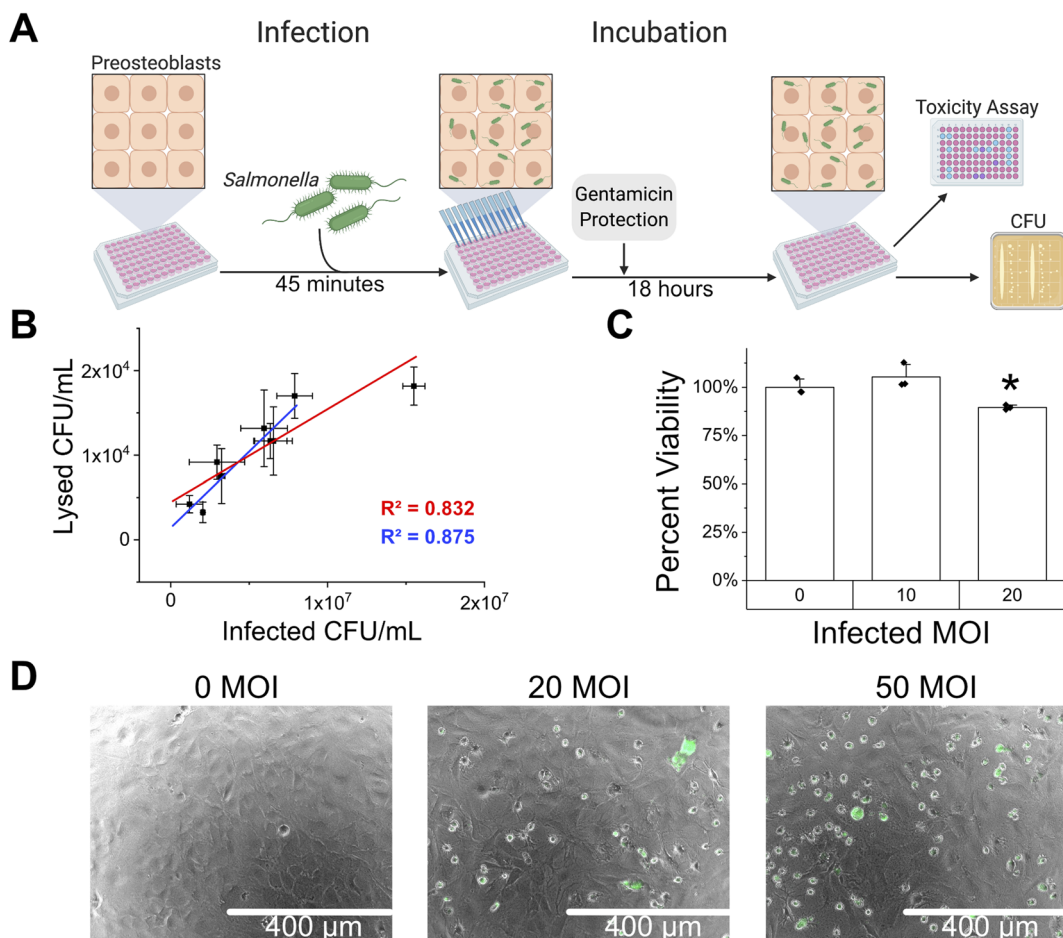


Fig. 3 Characterization of *Salmonella* intracellular infection of preosteoblast cells. (A) Schematic of *Salmonella* intracellular infection of preosteoblasts protocol. (B) Characterized linear trend of increasing infected CFU per mL compared to lysed intracellular load in CFU per mL. (C) Preosteoblast viability characterization with increasing CFU per mL using a lactate dehydrogenase (LDH) assay showing no statistical toxicity at 10 MOI (unpaired t-test, equal variance, $\alpha = 0.05$). (D) Brightfield images of preosteoblast cells infected with *Salmonella* expressing GFP (green) showing an increasing in GFP containing cells with an increase in infected MOI.

potentially reaching a saturation point (Fig. 3B). Microscopy also showed an increase in fluorescent intracellular GFP from SL1344 with increasing MOI (ESI Fig. S6†). Additionally, we determined the maximum MOI before affecting host cell viability by varying the MOI and measuring the amount of lactate dehydrogenase (LDH) released from damaged host cells. The LDH toxicity assay determined that an MOI of 10 does not affect host cell viability ($P = 0.78$, Fig. 3C). Finally, the intracellular infection was also visualized by microscopy aided by the fact that the *Salmonella* SL1344 expresses GFP from the chromosome. Increasing MOI also showed an increased number of infected preosteoblast cells, seen by increased GFP containing cells (Fig. 3D).

Following QD toxicity testing of *Salmonella* and the host cells individually, we measured the efficacy of intracellular infection treatment. The same protocol as for infection was followed except that CdTe-2.4 eV was added to the final media change before the 18 hour incubation and incubation was done under light activation (Fig. 4A). At all QD concentrations tested there was significant reductions of total intracellular bacteria load

while under light activation, shown through microscopy and intracellular CFU load. Visualization using microscopy also showed a dramatic decrease in intracellular GFP fluorescence, indicating a reduction of intracellular bacteria (Fig. 4B). The total intracellular load or percent infection, total bacteria in lysate normalized to no treatment, decreased with treatment to 40.3% (± 13.9), 18.1% (± 3.0), and 16.5% (± 5.2) for 100, 400, and 600 nM respectively (Fig. 4C and ESI Fig. S7,† two sample t-test, $P > 0.05$). Additionally, we varied the MOI to see if a decreased burden of infection would be easier to treat. Treating with 100 nM CdTe-2.4 showed a decrease in intracellular infection loads across all MOIs but maintained a similarly proportioned intracellular load to no treatment. However, at 600 nM CdTe-2.4 eV while all MOIs show a drop in intracellular load compared to no treatment at the lower MOIs, 1 and 5 MOI, there is no longer a statistical difference in the intracellular load indicating that treatment is more effective at lower MOIs (Fig. 4D).

Light activated nanoparticles are advantageous in that they can be spatially and temporally modulated based on the

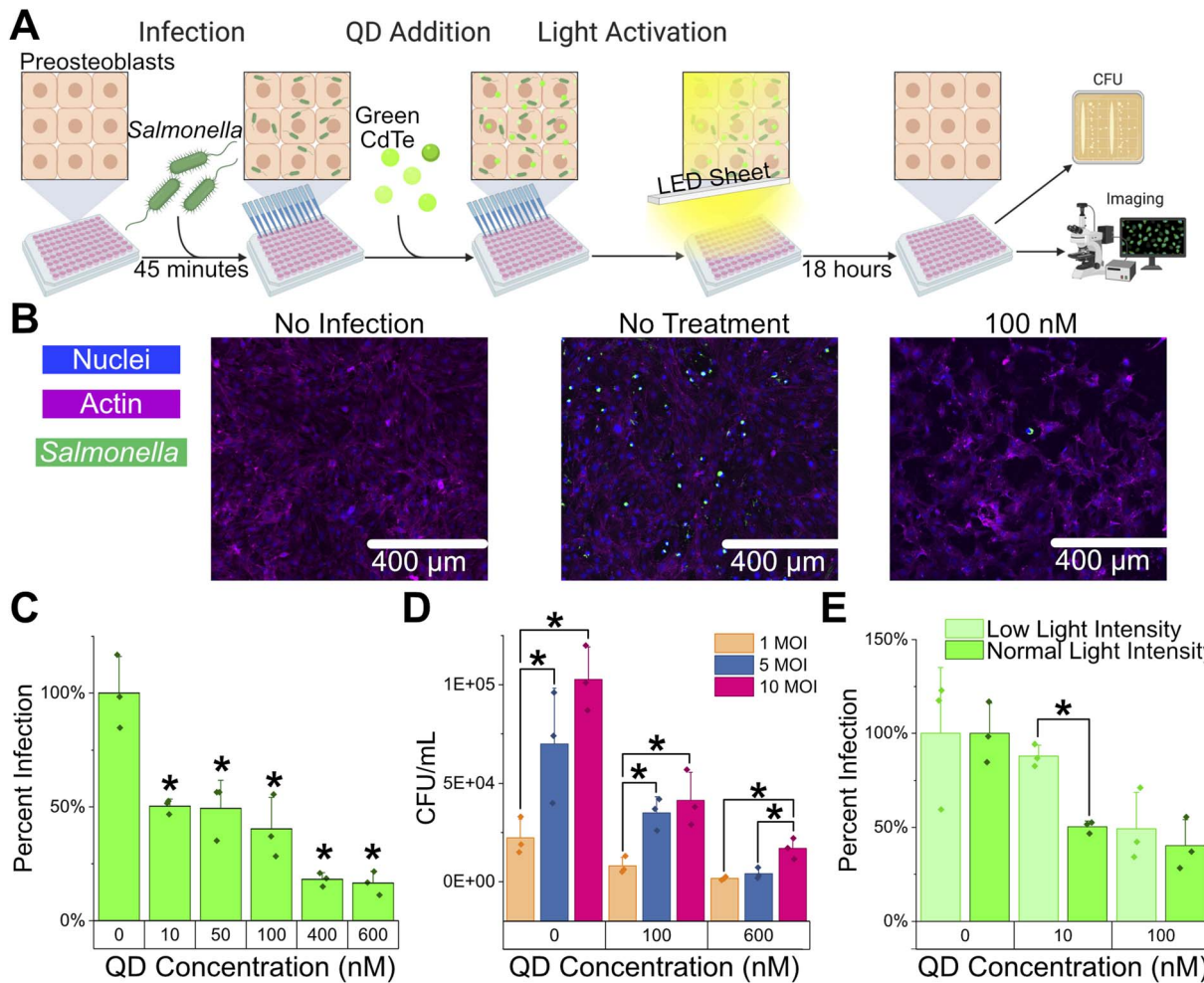


Fig. 4 Treatment of intracellular infection of *Salmonella* by light activated CdTe-2.4 eV nanoparticles. (A) Infection and treatment schematic of *Salmonella* intracellular infection of preosteoblasts treated with light activated CdTe-2.4 eV. (B) Confocal microscopy images of preosteoblasts stained with Dapi (blue, nuclei) and phalloidin 647 (magenta, actin) and *Salmonella* expressing GFP (green). No infection shows no GFP fluorescence and no treatment compared to 100 nM CdTe-2.4 eV treatment shows a significant reduction in GFP at 10 MOI. (C) Percent infection (normalized lysed CFU per mL of each treatment condition to the lysed CFU per mL of the no treatment condition) at various treatment conditions showing statistically significant reduction in percent infection at all treatment concentrations (unpaired *t*-test, equal variance, $\alpha = 0.05$). (D) Lysed CFU per mL of CdTe-2.4 eV treatment of intracellular infection at varying MOIs. The intracellular load of 1 MOI was statistically different to 5 and 10 MOI, as such the final intracellular load after 100 nM treatment for 1 MOI was also statistically different to 5 and 10 MOI. 5 and 10 MOI were not statistically different to each other at 0 nM or 100 nM treatment. At 600 nM the intracellular load of 1 and 5 MOI are no longer statistically different but now 10 MOI is statistically different from 1 and 5 MOI. (E) Percent infection of 10 MOI *Salmonella* intracellular infection with CdTe 2.4 eV treatment at varying concentration and light intensity, low intensity at 67% of normal intensity. All statistics were done using an unpaired *t*-test assuming equal variance ($\alpha = 0.05$).

location and severity of infection. Light intensity directly correlates with nanoparticle activation and superoxide production creating further personalization.²² With the same visible white light ($\sim 450\text{--}550$ nm) as was used for activation of the CdTe-2.4 eV QDs, we tested the effect of light intensity modulation to determine if there is a correlated effect on treatment efficacy. With a decreased light intensity (67% of previous light intensity, ESI Fig. S8†) there is similar clearance of an intracellular infection at 100 nM, but a statistically insignificant decrease in clearance at 10 nM for low light intensity as compared to normal light intensity (Fig. 4E and ESI Fig. S9†).

Here, we introduced foundational work for a new approach to the treatment of intracellular bacterial infection. Our CdTe-2.4 eV QDs effectively inhibited growth of *Salmonella* Typhimurium in broth culture due to specific production of superoxide ROS. QDs without photoactivation showed minimal effect on bacterial growth (Fig. 1D and F, ESI Fig. S2†) and QDs tuned to a 2.2 eV bandgap, which do not specifically produce superoxide, were less effective in inhibiting growth compared to 2.4 eV QDs (Fig. 1E and G, ESI Fig. S2†). Though some inhibition of *Salmonella* growth was observed in the presence of these 2.2 eV QDs, this may be attributed to the larger spread of QDs present in the 2.2 eV QD samples (ESI Fig. S1†). As the 2.2 eV QDs were synthesized by increasing thermal reaction time, the



spread in QD diameter was larger, resulting in a range of QD sizes averaging a bandgap of 2.2 eV. Thus, a fraction of the QDs would still be able to produce superoxide when activated by light (Fig. 1B), leading to the less pronounced but statistically significant decrease in *Salmonella* growth. Note that the 2.4 eV QDs require a shorter thermal reaction time, therefore the spread in size and bandgap of these QDs is considerably narrower.

While both 400 nM and 600 nM concentrations of CdTe-2.4 eV QDs was sufficient to inhibit *Salmonella* growth by more than 50% of control, no toxicity was observed at these concentrations in preosteoblast cells (Fig. 2B, ESI Fig. S4†) measured by a Resazurin Viability Assay. A QD concentration of 1 μ M caused toxicity, though it did not completely kill all preosteoblast cells. As such, we proceeded with testing ranges of QD concentrations up to 600 nM against intracellular infections. Note that while resazurin showed a convincing lack of toxicity at 600 nM and below (Fig. 2B), LDH assays did not give conclusive results. This may be due to the nature of the positive control in the LDH assay, which is lysing of cells with Triton-X, compared to that in the resazurin assay, which is addition of no cells. This results in larger variability of the positive control in the LDH assay where potentially not all cells are dead.

A low MOI was chosen for infection of preosteoblast cells with *Salmonella* Typhimurium to ensure linearity between infection CFU per mL and CFU per mL post-lysis (Fig. 3B). Additionally, 10 MOI did not cause toxicity to the preosteoblast cells, while higher MOI led to decreased viability of preosteoblast cells (Fig. 3C). Higher MOI was directly correlated to higher number of infected cells (Fig. 3B and D, ESI Fig. S6†), rather than just increasing severity of infection in a small population of cells, therefore we could reliably expect that MOI used at the start of the infection would predict final count of infected cells after incubation.

Intracellular infection of *Salmonella* Typhimurium in preosteoblast cells were successfully treated using CdTe-2.4 eV QDs (Fig. 4C and ESI Fig. S7†). Increased QD concentration resulted in decreased final CFU of intracellular bacteria, with significant decrease in infection observed at QD concentrations of 10 nM and above. Degree of infection was visually confirmed by imaging the GFP-expressing *Salmonella*. Treatment with QDs led to fewer infected cells (Fig. 4B). The CdTe-2.4 eV QDs were also tested against lower MOI infections, showing that the clearance of infection was not decreased when MOI was increased from 1 to 5 or 10. At 600 nM, though lower MOIs have little remaining bacteria and there is no difference between 1 and 5 MOI, there is still a difference between low MOIs (1 and 5) and a high MOI (10), showing that it is easier to clear a lower MOI infection. Higher MOI conditions were not tested, as higher than 10 MOI resulted in decreased viability of host cells (Fig. 3B) which could confound results.

The effect of varying light intensity on QD efficacy was also explored. While 100 nM QD showed no difference regardless of low or high light intensity (ESI Fig. S8 and S9†) we observed a decrease in the effect of lower QD concentrations on infection when light was kept at low intensity. Higher light intensity was not tested due to the negative effects of heating on mammalian

cells. This confirms the dependence of this treatment on photoactivation.

While intracellular bacterial infections are traditionally hard to treat due to the multiple barriers that antibiotics must cross to reach the invading pathogens, our CdTe-2.4 eV QDs are able to effectively mitigate intracellular infections even at low dosage concentrations. The decrease in bacterial load because of CdTe-2.4 eV QD treatment may be sufficient to enable host immune response to clear osteomyelitis infection. Additionally, previous work shows that QDs synergize with conventional antibiotics, suggesting combination therapy as an option for particularly severe infections or immunocompromised patients.²² In cultured mammalian cells, the upper limit before seeing significant toxicity was seen to be about 1 μ M, but in an *in vivo* setting, localized higher doses may be possible. Higher light intensities would also be possible in an *in vivo* setting as slight heating from the LEDs would not be as detrimental as they are for mammalian cells *in vitro*. Further exploration into the efficacy of the QDs against a variety of intracellularly infecting strains of bacteria and infected mammalian cell types would better characterize the full capabilities of this treatment.

This treatment displays how superoxide producing nanoparticles can effectively treat an intracellular infection. The spatial and temporal tunability of this therapeutic means it can be adapted to treat various infections and the small size of the nanoparticles allow it to transport into hard-to-reach areas. While a treatment that is dependent upon visible light activation does not translate well to a therapeutic for deep bone infection, the work presented here lays a foundation for treatment of superficial intracellular infections in which QDs can be activated with visible light. Furthermore, we have recently developed superoxide producing nanoparticles that are activated by near infrared light which penetrates tissues better.²⁰ Future work will be done on developing superoxide producing nanoparticles activated by further penetrating stimuli such as ultrasound.

Here we have established and characterized an intracellular infection of *Salmonella* in preosteoblast cells as well as validated the effective treatment of *Salmonella* extracellularly and intracellularly using superoxide producing, light activated nanoparticles. We've shown how light modulation directly correlates to infection clearance and can be tuned based on infection severity. We have also shown an increased therapeutic efficacy at lower MOIs.

Materials and methods

QD synthesis and filtration

CdTe-2.4 eV and CdTe 2.2 eV QDs were synthesized as described previously in Courtney *et al.* 2016. Briefly, the cadmium precursor was made by combining CdCl₂ (0.4 mg mL⁻¹; Sigma) and 3-mercaptopropionic acid (1 mg mL⁻¹; Fischer) in degassed, double distilled water (DDW). An equal volume of cadmium precursor and degassed DDW were added to 0.5 M NaOH (0.2% total volume) and NaHTe (40 mg mL⁻¹, 0.2% total volume) to make the unreacted CdTe precursor solution. The precursor solution was stored at 4 °C, sealed and protected from

light for up to a month. CdTe was reacted on the same day as it was used by splitting into 500 μ L aliquots and reacting at 98 °C until the desired size, 2.4 eV or 2.2 eV, was achieved. Sterile supplies and procedure was used throughout. The QDs were then filtered and washed in 200 μ L batches to remove any unreacted starting material using 100 μ L sterile pH 11 for rinses in a sterilized 4 K Nanosep filter (Pall) and centrifuging at 10k rpm for 7 minutes for each filter and wash step. QD were washed thrice and redispersed in 100 μ L pH 11 water. QD concentration was determined by acquiring ultraviolet-visible spectra using a VWR UV1600-PC spectrophotometer at 1 nm resolution and calculating the concentration with optical concentration correlations.³⁶

EPR superoxide characterization

Nanoparticles were synthesized, filtered, and washed as described above except final redispersion was done in DDW and supplemented with DMPO (1 vol%; Dojindo). Samples were kept in dark conditions as much as possible before testing. EPR spectra was acquired using a Bruker Elexsys E 500 spectrometer with an SHQE cavity at 7 mW microwave intensity. Samples were loaded into four quartz capillaries and first measured in dark for a baseline and then measured with 365 nm light for 30 s for each scan. Ten scans were done and the normalized superoxide was calculated by taking the average of the ten scans and normalizing to the average of the CdTe-2.4 eV ten scans. Normalized superoxide production for CdTe-2.2 eV was determined by first calculating the relative superoxide production of CdTe-2.2 eV compared to CdTe-2.4 eV while accounting for difference in concentrations, using eqn (1) where EPR is the average over 10 scans and A is the area under the absorbance curve from UV-vis from 400 nm to 800 nm, and then normalizing to the average of the CdTe-2.4 eV ten scans.

$$\text{Relative superoxide production} = \frac{\text{EPR}_{\text{CdTe-2.2 eV}} \times A_{\text{CdTe-2.4 eV}}}{A_{\text{CdTe-2.2 eV}}} \quad (1)$$

Bacterial cell culture

Bacterial cultures were maintained long-term in Lysogeny Broth (LB, Sigma-Aldrich) media with 40% glycerol at -80 °C. SL1344 was cultured in LB supplemented with streptomycin (30 μ g mL⁻¹ liquid culture, 40 μ g mL⁻¹ solid media, Sigma-Aldrich). From a freezer stock, bacteria were streaked onto solid media and overnight cultures inoculated from individual colonies off of solid media and grown for 16 hours at 37 °C with shaking.

Osteoblast cell culture

MC3T3-E1 pre-osteoblast cells (ATCC, CRL 2593) were seeded at passage 8 from long-term storage, 10% DMSO and full growth media in liquid nitrogen. MC3T3-E1 cells were maintained at sub-confluent density in full growth media, Minimum Essential Media (MEM) Alpha (Gibco) supplemented with 10% Fetal Bovine Serum (Atlanta Biologics) and 1% antibiotics (5000 units

per mL penicillin, 500 μ g mL⁻¹ streptomycin, hyclone), at 37 °C, 5% CO₂, and humidity. Once recovered from a freezer stock, cells were passaged into three separate flasks, maintained and subcultured as separate biological replicates for all experiments. In all 96 well plate experiments, unless otherwise indicated, MC3T3-E1 cells were seeded into 96 well plates at 10 000 cells per well in 100 μ L of full growth media and allowed to adhere for 24 hours prior to experiment.

QD toxicity in osteoblasts

QDs were serially diluted into full growth media and allowed to adhere for 24 hours. After 24 hours media was replaced with QD containing media and incubated in light or dark conditions for 18 hours. For the Lactate Dehydrogenase (LDH) cytotoxicity assay (CytoSelect™ LDH Cytotoxicity Assay Kit, Cell Biolabs) manufacturer protocol was followed, briefly 50 μ L of sterile double distilled water was added to the supernatant and 100 μ L of the supernatant solution was transferred to a new 96 well plate. The supernatant was reacted with the LDH cytotoxicity assay reagent for 30 minutes at 37 °C and 5% CO₂. Absorbance was read at 450 nm and background subtracted. Percent toxicity was calculated using eqn (2). For the resazurin viability assay cell seeding, culture, and treatment were done in the same way as the LDH assay. Following 18 hours of treatment media was exchanged with full growth media containing 44 μ M resazurin sodium salt (Sigma-Aldrich) and incubated at growth conditions for 3–4 hours then fluorescence measured using excitation at 560 nm and emission at 590 nm. Percent viability was calculated using eqn (3) where FI is fluorescence intensity at 590 nm emission (560 nm excitation) and percent toxicity was calculated as the inverse.

$$\text{Percent toxicity} = \frac{\text{absorbance}_{450 \text{ nm}}^{\text{treatment}} - \text{absorbance}_{450 \text{ nm}}^{\text{no treatment}}}{\text{absorbance}_{450 \text{ nm}}^{\text{positive control}} - \text{absorbance}_{450 \text{ nm}}^{\text{no treatment}}} \quad (2)$$

$$\text{Percent viability} = \frac{\text{FI}_{\text{Em 590 nm}}^{\text{treatment}} - \text{FI}_{\text{Em 590 nm}}^{\text{positive control}}}{\text{FI}_{\text{Em 590 nm}}^{\text{no treatment}} - \text{FI}_{\text{Em 590 nm}}^{\text{positive control}}} \quad (3)$$

Salmonella infection characterization & QD treatment

SL1344 was grown overnight (16 hours) in LB containing streptomycin, diluted 1:10 in 5 mL of LB, and grown for 3 hours. Following regrowth, bacteria was rinsed in PBS twice, to remove remaining antibiotic, and a final rinse and resuspension performed in DPBS. OD_{600nm} was measured, with media subtracted, to determine the CFU per mL and bacteria was diluted into DPBS to the desired MOI based on 10 000 osteoblast cells per well. Prior to infection, osteoblast cells were rinsed twice in DPBS then infected with 100 μ L of DPBS containing bacteria per well. Osteoblasts were infected for 45 minutes then media was replaced with MEM- α containing 10% FBS and 100 μ g mL⁻¹ gentamycin to remove any remaining extracellular bacteria and incubated for 75 minutes. A final media replacement was done with the same growth media but



with $10 \mu\text{g mL}^{-1}$ gentamycin and treatment when appropriate and incubated for 18 hours, with light illumination using LED sheet when appropriate. Toxicity was measured using by LDH assay using the protocol as described above for QD toxicity testing.

Additionally, preosteoblast cells were infected at varying MOI, infection protocol followed as above, and incubated for 18 hours. Following incubation the preosteoblast cells were washed thrice with DPBS to remove gentamicin in the media and lysed with $30 \mu\text{L}$ of 0.1% Triton-X100 (Sigma-Aldrich) for 15 minutes at room temperature. Triton was diluted 10-fold by $270 \mu\text{L}$ addition of DPBS and full lysis was ensured by additional pipetting. Lysate was then serially diluted and $10 \mu\text{L}$ plated to enumerate CFU. Further, intracellular infection was visualized by microscopy using brightfield for the preosteoblast cells and GFP for the bacteria.

Staining and visualization

Post treatment osteoblast cells were washed thrice with DPBS and fixed in 3.7% methanol free formaldehyde (Sigma-Aldrich) for 20 minutes at room temperature and subsequently rinsed thrice with DPBS. DAPI was diluted to 2.5 ng mL^{-1} in DPBS, $100 \mu\text{L}$ added to each well, and incubated at room temperature for 5 minutes. Prior to staining with Phalloidin 647 cells were rinsed twice with DPBS then stained with $100 \mu\text{L}$ of 165 nM Phalloidin 647 solution containing 0.25% Triton-X-100 for 20 minutes at room temperature. Cells were rinsed with DPBS twice and imaged in PBS. DAPI, Phalloidin 647, and GFP were imaged using Ex: 375/28 nm and Em: 460/60 nm, Ex: 620/50 nm and Em: 690/50 nm, and Ex: 480/30 nm and Em: 535/45 nm respectively.

Statistical analysis

Statistical analysis was done in Excel by performing an unpaired, two-sided *t*-test with an α of 0.05 unless otherwise stated. Biological replicates of 3 were always done unless otherwise noted and sample standard deviation is shown in figures. Regression analysis for linear fits was done in Minitab.

Author contributions

K. A. E., C. R. M., J. K. C., M. L., K. A. E., P. N. and A. C. designed the experiments. K. A. E. conducted all experiments. M. L. performed nanoparticle EPR analysis. A. C., K. A. E., C. R. M., D. F. S., P. N., and J. K. C. analyzed all experimental data. A. C., K. A. E., D. F. S., and C. R. M. wrote the paper. All the authors discussed the results and edited the manuscript.

Conflicts of interest

The authors declare no competing financial interests.

Acknowledgements

We acknowledge financial support from W. M. Keck Foundation and DARPA Young Faculty Award (D17AP00024) to A. C. and

National Aeronautics and Space Administration (NASA) Cooperative Agreement Notice – Translational Research Institute (TRISH) award number NNX16A069A to A. C. and P. N. The authors would like to acknowledge the Department of Education's Graduate Assistantship in Areas of National Need to CRM. The views, opinions, and findings contained in this article are those of the author and/or should not be interpreted as representing the official views or policies, either expressed or implied, of the Defense Advanced Research Projects Agency or the Department of Defense. All data needed to evaluate the conclusions in the paper are present in the paper and/or the Supplementary Materials. Additional data available from authors upon request.

References

- 1 C. L. Ventola, The antibiotic resistance crisis: part 1: causes and threats, *Pharm. Ther.*, 2015, **40**, 277–283.
- 2 E. Martens and A. L. Demain, The antibiotic resistance crisis, with a focus on the United States, *J. Antibiot.*, 2017, **70**, 520–526.
- 3 K. H. Luepke, *et al.*, Past, Present, and Future of Antibacterial Economics: Increasing Bacterial Resistance, Limited Antibiotic Pipeline, and Societal Implications, *Pharmacother. J. Hum. Pharmacol. Drug Ther.*, 2017, **37**, 71–84.
- 4 U. Theuretzbacher, K. Outterson, A. Engel and A. Karlén, The global preclinical antibacterial pipeline, *Nat. Rev. Microbiol.*, 2019, 1–11, DOI: [10.1038/s41579-019-0288-0](https://doi.org/10.1038/s41579-019-0288-0).
- 5 R. Laxminarayan, *et al.*, The Lancet Infectious Diseases Commission on antimicrobial resistance: 6 years later, *Lancet Infect. Dis.*, 2020, **20**, e51–e60.
- 6 CDC, *Antibiotic Resistance Threats in the United States, 2019*, U.S. Department of Health and Human Services, 2019, DOI: [10.15620/cdc:82532](https://doi.org/10.15620/cdc:82532), <https://stacks.cdc.gov/view/cdc/82532>.
- 7 N. F. Kamaruzzaman, S. Kendall and L. Good, Targeting the hard to reach: challenges and novel strategies in the treatment of intracellular bacterial infections, *Br. J. Pharmacol.*, 2017, **174**, 2225–2236.
- 8 P. M. Tulkens, Intracellular distribution and activity of antibiotics, *Eur. J. Clin. Microbiol. Infect. Dis.*, 1991, **10**, 100–106.
- 9 M. Barcia-Macay, C. Seral, M.-P. Mingeot-Leclercq, P. M. Tulkens and F. Van Bambeke, Pharmacodynamic evaluation of the intracellular activities of antibiotics against *Staphylococcus aureus* in a model of THP-1 macrophages, *Antimicrob. Agents Chemother.*, 2006, **50**, 841–851.
- 10 H. J. Forman and M. Torres, Reactive oxygen species and cell signaling: respiratory burst in macrophage signaling, *Am. J. Respir. Crit. Care Med.*, 2002, **166**, S4–S8.
- 11 C. N. Paiva and M. T. Bozza, Are Reactive Oxygen Species Always Detrimental to Pathogens?, *Antioxid. Redox Signaling*, 2014, **20**, 1000–1037.
- 12 E. Cabisco Catala, J. Tamarit Sumalla and J. Ros Salvador, Oxidative stress in bacteria and protein damage by reactive oxygen species, *Int. Microbiol.*, 2000, **3**, 3–8.



13 J. A. Imlay, Pathways of Oxidative Damage, *Annu. Rev. Microbiol.*, 2003, **57**, 395–418.

14 U. Bandyopadhyay, D. Das and R. K. Banerjee, Reactive oxygen species: oxidative damage and pathogenesis, *Curr. Sci.*, 1999, **77**, 658–666.

15 H. Van Acker and T. Coenye, The Role of Reactive Oxygen Species in Antibiotic-Mediated Killing of Bacteria, *Trends Microbiol.*, 2017, **25**, 456–466.

16 C. E. Probst, P. Zrazhevskiy, V. Bagalkot and X. Gao, Quantum dots as a platform for nanoparticle drug delivery vehicle design, *Adv. Drug Delivery Rev.*, 2013, **65**, 703–718.

17 S. Xie, *et al.*, Biodegradable nanoparticles for intracellular delivery of antimicrobial agents, *J. Controlled Release*, 2014, **187**, 101–117.

18 N. Abed and P. Couvreur, Nanocarriers for antibiotics: a promising solution to treat intracellular bacterial infections, *Int. J. Antimicrob. Agents*, 2014, **43**, 485–496.

19 M. Levy, *et al.*, Assessing different reactive oxygen species as potential antibiotics: selectivity of intracellular superoxide generation using quantum dots, *ACS Appl. Bio Mater.*, 2018, **1**, 529–537.

20 M. Levy, J. R. Bertram, K. A. Eller, A. Chatterjee and P. Nagpal, Near-Infrared-Light-Triggered Antimicrobial Indium Phosphide Quantum Dots, *Angew. Chem., Int. Ed.*, 2019, **58**, 11414–11418.

21 M. Levy, P. P. Chowdhury, K. A. Eller, A. Chatterjee and P. Nagpal, Tuning Ternary $Zn_{1-x}Cd_xTe$ Quantum Dot Composition: Engineering Electronic States for Light-Activated Superoxide Generation as a Therapeutic against Multidrug-Resistant Bacteria, *ACS Biomater. Sci. Eng.*, 2019, **5**, 3111–3118.

22 C. M. Courtney, *et al.*, Potentiating antibiotics in drug-resistant clinical isolates *via* stimuli-activated superoxide generation, *Sci. Adv.*, 2017, **3**, e1701776.

23 C. M. Courtney, *et al.*, Photoexcited quantum dots for killing multidrug-resistant bacteria, *Nat. Mater.*, 2016, **15**, 529.

24 C. R. Mccollum, M. Levy, J. R. Bertram, P. Nagpal and A. Chatterjee, Photoexcited Quantum Dots as Efficacious and Nontoxic Antibiotics in an Animal Model, *ACS Biomater. Sci. Eng.*, 2021, **7**, 1863–1875.

25 M. A. El-Sayed, Small is different: Shape-, size-, and composition-dependent properties of some colloidal semiconductor nanocrystals, *Acc. Chem. Res.*, 2004, **37**, 326–333.

26 S. M. Goodman, *et al.*, Designing Superoxide-Generating Quantum Dots for Selective Light-Activated Nanotherapy, *Front. Chem.*, 2018, **6**, 46.

27 M. Levy, P. P. Chowdhury and P. Nagpal, Quantum dot therapeutics: a new class of radical therapies, *J. Biol. Eng.*, 2019, **13**, 48.

28 M. Levy, J. R. Bertram, K. A. Eller, A. Chatterjee and P. Nagpal, Near-Infrared Light Triggered Antimicrobial Indium Phosphide Quantum Dots, *Angew. Chem., Int. Ed.*, 2019, **58**, 11414–11418.

29 T. R. Aunins, *et al.*, Isolating the *Escherichia coli* Transcriptomic Response to Superoxide Generation from Cadmium Chalcogenide Quantum Dots, *ACS Biomater. Sci. Eng.*, 2019, **5**, 4206–4218.

30 C. M. Courtney, *et al.*, Potentiating clinical drug resistant bacteria *via* stimuli-activated superoxide generation, *Sci. Adv.*, 2017, **3**, e1701776.

31 S. Chihara and J. Segreli, Osteomyelitis, *DM, Dis.-Mon.*, 2010, **56**, 6–31.

32 D. P. Lew and F. A. Waldvogel, Osteomyelitis, *Lancet*, 2004, **364**, 369–379.

33 I. Marriott, Osteoblast responses to bacterial pathogens: a previously unappreciated role for bone-forming cells in host defense and disease progression, *Immunol. Res.*, 2004, **30**, 291–308.

34 E. H. Alexander, *et al.*, *Staphylococcus aureus* and *Salmonella enterica* serovar *dublin* induce tumor necrosis factor-related apoptosis-inducing ligand expression by normal mouse and human osteoblasts, *Infect. Immun.*, 2001, **69**, 1581–1586.

35 P. Vaudaux and F. A. Waldvogel, Gentamicin Antibacterial Activity in the Presence of Human Polymorphonuclear Leukocytes, *Antimicrob. Agents Chemother.*, 1979, **16**, 743–749.

36 W. W. Yu, L. Qu, W. Guo and X. Peng, Experimental determination of the extinction coefficient of CdTe, CdSe, and CdS nanocrystals, *Chem. Mater.*, 2003, **15**, 2854–2860.

